

# The eisosome core is composed of BAR domain proteins

Agustina Olivera-Couto, Martin Graña, Laura Harispe, and Pablo S. Aguilar  
 Institut Pasteur de Montevideo, Montevideo 11400, Uruguay

**ABSTRACT** Eisosomes define sites of plasma membrane organization. In *Saccharomyces cerevisiae*, eisosomes delimit furrow-like plasma membrane invaginations that concentrate sterols, transporters, and signaling molecules. Eisosomes are static macromolecular assemblies composed of cytoplasmic proteins, most of which have no known function. In this study, we used a bioinformatics approach to analyze a set of 20 eisosome proteins. We found that the core components of eisosomes, paralogue proteins Pil1 and Lsp1, are distant homologues of membrane-sculpting Bin/amphiphysin/Rvs (BAR) proteins. Consistent with this finding, purified recombinant Pil1 and Lsp1 tubulated liposomes and formed tubules when the proteins were overexpressed in mammalian cells. Structural homology modeling and site-directed mutagenesis indicate that Pil1 positively charged surface patches are needed for membrane binding and liposome tubulation. Pil1 BAR domain mutants were defective in both eisosome assembly and plasma membrane domain organization. In addition, we found that eisosome-associated proteins Slm1 and Slm2 have F-BAR domains and that these domains are needed for targeting to furrow-like plasma membrane invaginations. Our results support a model in which BAR domain protein-mediated membrane bending leads to clustering of lipids and proteins within the plasma membrane.

## Monitoring Editor

David G. Drubin  
 University of California,  
 Berkeley

Received: Jan 3, 2011

Revised: May 2, 2011

Accepted: May 6, 2011

## INTRODUCTION

As the cellular border, the plasma membrane manages the traffic of materials and information into and out of the cell. To cope with so many diverse tasks, the plasma membrane is organized into dynamic compartments or domains where different components and functions take place. These domains exist over a wide range of spatial and temporal scales, ranging from nanometers to micrometers and from milliseconds to highly stable or even static domains (Lingwood and Simons, 2010). Extensively studied examples of micrometer-scale organization include epithelial cells, where the apical and basolateral domains of the plasma membrane segregate a large set of specific proteins and lipids (Tanos and Rodriguez-Boulan, 2008). Below the micrometer level, nanoscale associations of lipids

and proteins modulate the spatial distribution of plasma membrane functions, including signal transduction, exocytosis, and endocytosis. Despite being extensively characterized, current understanding of submicrometer plasma membrane domain biogenesis remains limited (Munro, 2003; Lingwood and Simons, 2010). The emerging picture involves a complex interplay among several different mechanisms. Lipids with self-associating properties (e.g., sterols and sphingolipids) congregate to provide lipidic platforms where certain proteins (e.g., glycosylphosphatidylinositol-anchored proteins) partition (Lingwood and Simons, 2010). Within the lipid bilayer, homotypic and heterotypic protein-protein interactions also segregate lipids by virtue of favored protein-lipid interactions (Poveda *et al.*, 2008). A third mechanism is provided by water-soluble components such as scaffolding proteins that are able to locally modify plasma membrane composition and topography by protein-protein and protein-lipid interactions (Johannes and Mayor, 2010; Lingwood and Simons, 2010).

Submicrometer domain organization is evident in the plasma membrane of *Saccharomyces cerevisiae*. Three plasma membrane domains have been described that were named after fluorescently tagged marker proteins used in various studies. The membrane compartment containing Can1 (MCC); the membrane compartment containing the target of rapamycin complex 2 (TORC2) or MCT, and the membrane compartment containing Pma1 (MCP) (Young *et al.*,

This article was published online ahead of print in MBoC in Press (<http://www.molbiolcell.org/cgi/doi/10.1091/mbc.E10-12-1021>) on May 18, 2011.

Address correspondence to: Pablo S. Aguilar ([pablo.aguilar@pasteur.edu.uy](mailto:pablo.aguilar@pasteur.edu.uy)).

Abbreviations used: BAR, Bin/amphiphysin/Rvs; MCC, membrane compartment containing Can1; MCP, membrane compartment containing Pma1; MCT, membrane compartment containing TORC2; PI(4,5)P<sub>2</sub>, L- $\alpha$ -phosphatidylinositol-4,5-bisphosphate; TORC2, target of rapamycin complex 2.

© 2011 Olivera-Couto *et al.* This article is distributed by The American Society for Cell Biology under license from the author(s). Two months after publication it is available to the public under an Attribution-Noncommercial-Share Alike 3.0 Unported Creative Commons License (<http://creativecommons.org/licenses/by-nc-sa/3.0>).

"ASCB," "The American Society for Cell Biology," and "Molecular Biology of the Cell" are registered trademarks of The American Society of Cell Biology.

ORF	Name	Evidence	Reference
Ygr086w	Pil1	Core component	Walther <i>et al.</i> , 2006
Ypl004c	Lsp1	Core component	Walther <i>et al.</i> , 2006
Ygr130c	Ygr130c	AC/MS, colocalization	Grossmann <i>et al.</i> , 2008; Deng <i>et al.</i> , 2009
Ymr031c	Eis1	AC/MS, colocalization	Grossmann <i>et al.</i> , 2008; Deng <i>et al.</i> , 2009; Aguilar <i>et al.</i> , 2010
Ymr086w	Ymr086w	AC/MS, colocalization	Krogan <i>et al.</i> , 2006; Deng <i>et al.</i> , 2009
Ynl173c	Mdg1	Colocalization	Grossmann <i>et al.</i> , 2008
Ydr490c	Pkh1	AC/MS, colocalization, functional	Zhang <i>et al.</i> , 2004; Walther <i>et al.</i> , 2007
Yol100w	Pkh2	AC/MS, colocalization, functional	Zhang <i>et al.</i> , 2004; Walther <i>et al.</i> , 2007
Ydr032c	Pst2	Colocalization	Grossmann <i>et al.</i> , 2008
Ybr052c	Rfs1	AC/MS, colocalization	Grossmann <i>et al.</i> , 2008
Ycr004c	Ycp4	AC/MS, colocalization	Grossmann <i>et al.</i> , 2008; Deng <i>et al.</i> , 2009
Yil105c	Slm1	Colocalization	Grossmann <i>et al.</i> , 2008
Ynl047c	Slm2	Colocalization	Grossmann <i>et al.</i> , 2008
Ypr115w	Rgc1	AC/MS	Krogan <i>et al.</i> , 2006
Ybr108w	Aim3	AC/MS	Krogan <i>et al.</i> , 2006
Ykl142w	Mrp8	AC/MS, Y2H	Ito <i>et al.</i> , 2001; Collins <i>et al.</i> , 2007; Yu <i>et al.</i> , 2008
Yer047c	Sap1	Y2H	Yu <i>et al.</i> , 2008
Ypl074w	Yta6	AC/MS	Ho <i>et al.</i> , 2002
Ylr219w	Msc3	Y2H, functional	Yu <i>et al.</i> , 2008; Moreira <i>et al.</i> , 2009

Paralogue proteins with no evidence for eisosome association are not listed. AC/MS, affinity chromatography/mass spectrometry; Y2H, yeast two-hybrid.

**TABLE 1: Analyzed eisosome-related proteins.**

2002; Malinska *et al.*, 2003; Berchtold and Walther, 2009). MCCs and MCTs are discrete foci, whereas the MCP is a continuous domain interrupted by MCCs and MCTs and otherwise occupies the rest of the plasma membrane. So far, the best-characterized domains are MCCs. On average, each cell contains 40 MCCs that are homogeneously distributed throughout the plasma membrane. MCCs concentrate sterols and several integral membrane proteins (Young *et al.*, 2002; Grossmann *et al.*, 2007). MCCs are also topographically distinctive, in that they are furrow-like plasma membrane invaginations 50 nm deep and 200–300 nm in length (Stradalova *et al.*, 2009). Remarkably, MCCs are immobile once formed, as their positions are fixed and unperturbed by cell growth and division. A cellular structure termed the eisosome is found intimately associated with the cytoplasmic side of every MCC. Each eisosome is a large proteinaceous assembly that is composed mainly of thousands of copies of two paralogous proteins, Pil1 and Lsp1 (Walther *et al.*, 2006). Despite being almost identical as well as similar in abundance, these proteins have different roles in eisosome structure and biogenesis. In the absence of Pil1, a large fraction of Lsp1 does not attach to the plasma membrane and remains cytoplasmic. The fraction of Lsp1 that remains associated with the plasma membrane forms few clusters that are larger than normal and were designated “eisosome remnants.” In contrast, in the absence of Lsp1, eisosomes form normally with Pil1 (Walther *et al.*, 2006). MCC organization, in turn, depends on eisosome integrity. In *pil1Δ* cells, all MCC markers analyzed so far, including sterols, lose their characteristic punctate pattern and spread along the plasma membrane, eventually concentrating with eisosomes remnants (Walther *et al.*, 2006; Grossmann *et al.*, 2007, 2008). Moreover, *pil1Δ* cells lack furrow-like plasma membrane invaginations (Stradalova *et al.*, 2009). Thus eisosomes emerged as plasma membrane domain organizers, but

molecular mechanisms involved are still unknown. In recent years, the number of proteins shown to be physically linked to eisosomes has steadily increased (Grossmann *et al.*, 2008; Deng *et al.*, 2009; Frohlich *et al.*, 2009; Aguilar *et al.*, 2010). However, we still lack molecular insight into eisosome function(s), since most of the eisosome-related proteins reported have little, if any, functional annotation.

In this study, we designed and executed a comprehensive bioinformatics analysis of eisosome proteins. We succeeded in identifying many unreported functional domains, and we demonstrate that eisosome core components Pil1 and Lsp1 belong to the membrane-sculpting Bin/amphiphysin/Rvs (BAR) superfamily of proteins. We also found that eisosome-associated proteins Slm1 and Slm2 contain F-BAR domains that are necessary for targeting to eisosomes. Finally, we show that a functional Pil1 BAR domain is required for both eisosome assembly and plasma membrane domain organization.

## RESULTS

### Bioinformatics analysis of eisosome proteins

To gain insight into eisosome molecular function(s), we systematically analyzed a set of 20 eisosome-related proteins (Table 1). We selected structural components of eisosomes Pil1 and Lsp1 in addition to cytoplasmic proteins that colocalize or physically interact with Pil1 or Lsp1 (such as Pkh1 and Eis1). When present, we also included protein paralogues of those just noted (e.g., Rgc2). We first assessed the phylogenetic distribution of eisosome proteins, scanning the National Center for Biotechnology Information Reference Sequence database using the Basic Local Alignment Search Tool (BLAST) with default parameters (Altschul *et al.*, 1997). Most significant hits were restricted to fungi, suggesting that eisosomes may be confined to this kingdom. Homologues of core components, Pil1 and Lsp1, were present in the monophyletic group Dikarya but seem

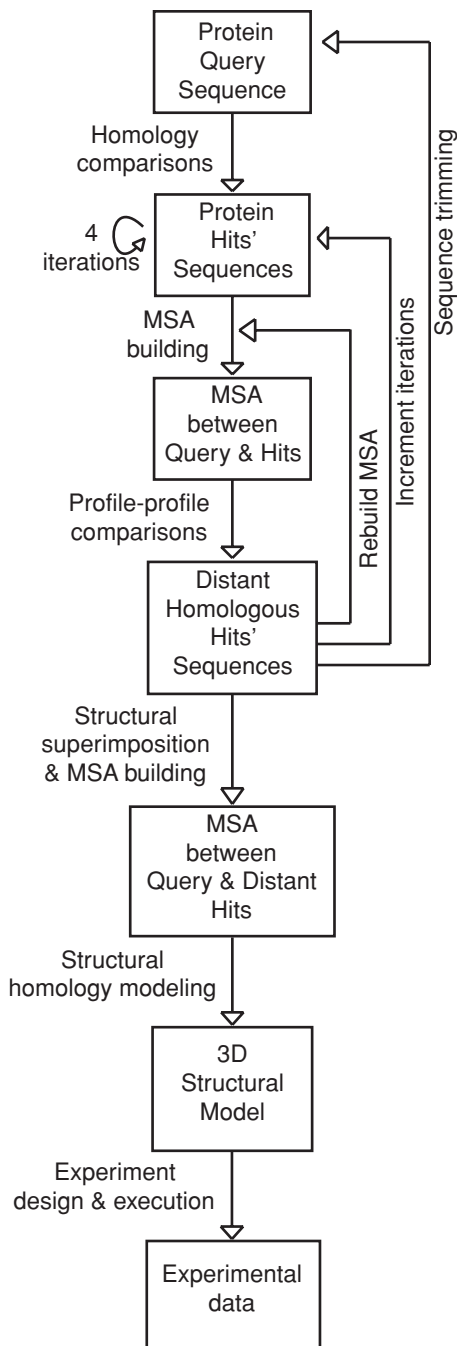


**FIGURE 1:** Bioinformatics pipeline. Protein sequence queries were subjected to homology comparisons using PSI-BLAST. Resulting hits were used to build MSAs, and then profile–profile comparisons were executed using both hidden Markov models–based algorithms (HHsearch) and COMPASS. Structure-based MSAs were then built using STAMP and T-Coffee and subsequently used for structure modeling. See *Materials and Methods* for details.

to be absent in Chytridiomycota, Microsporidia, and Mucoromycotina. Phylogenetic analyses of Pil1 and Lsp1 orthologues support a history of at least five independent duplications of an ancestral gene (Supplemental Figure S1). Evolutionary preservation of a molecular function does not necessarily rely on linear amino acid sequence similarities, so we also searched for conserved structural domains in the set of eisosome-related proteins. We designed a bioinformatics protocol consisting of exhaustive and iterative searches that gradu-

Name	Domain	Region (protein total length)
Pil1	BAR/N-BAR	53–214 (339)
Lsp1	BAR/N-BAR	53–214 (341)
Ygr130c	Coiled-coil	450–604 (816)
Eis1	Coiled-coil	447–676 (843)
Mdg1	Carbohydrate binding	8–71 (366)
	Carbohydrate binding	140–232 (366)
Pkh2	Pleckstrin homology	874–951 (1081)
Slm1	F-BAR	190–450 (686)
	Glutamine and asparagine rich	1–180 (686)
Slm2	F-BAR	166–426 (656)
	Glutamine and asparagine rich	1–120 (656)
Rgc1	F-BAR	157–461 (1083)
Rgc2	F-BAR	115–448 (1146)
Aim3	Glutamine and proline rich	31–320 (947)
Mrp8	Coiled-coil	7–116 (219)
Sap1	Coiled-coil	29–98 (897)
Yta6	Coiled-coil	22–250 (754)

**TABLE 2:** Protein domains found in distant homology analysis.

ally increased in sensitivity (see Figure 1 and *Materials and Methods* for details). Hits that were obtained with all algorithms used and that were consistent across all queries were considered as bona fide results (Table 2). Results obtained for the entire set are given in the supplemental materials. For certain queries (such as Msc3 and Ymr086w) this analysis did not yield reliable results, suggesting that some eisosome components harbor yet-unknown functional domains. Many of the remaining proteins had domains involved in protein–protein and protein–lipid interactions. We found the presence of BAR domains within Pil1, Lsp1, Slm1, Slm2, Rgc1, and Rgc2. The type of BAR domain found in Pil1 and Lsp1 was BAR/N-BAR, whereas in Slms and Rgcs putative F-BAR domains were evident. BAR domains are composed of three long  $\alpha$ -helices that dimerize into crescent-shaped modules with positively charged surfaces. These modules act as molecular scaffolds that bind to and bend negatively charged lipid membranes (Frost *et al.*, 2009). BAR domains define a superfamily of proteins composed of three different families: the BAR/N-BARs, the F-BARs, and the I-BARs. In BAR/N-BAR and F-BAR dimers the positively charged concave face is the membrane-binding interface. In contrast, the convex face of I-BAR dimers mediates membrane binding. As a general mechanism of action, the positively charged surface of the BAR dimer imposes its rigid shape on the engaged membrane and thereby bends it (Frost *et al.*, 2009). Thus our bioinformatics results are consistent with eisosomes being plasma membrane-associated structures and being required for the formation of furrow-like invaginations. Because our main objective was gaining insight into eisosome molecular function(s), we focused on its core components, Pil1 and Lsp1.

### Pil1 and Lsp1 harbor BAR domains

The alignments resulting from profile–profile comparisons including Pil1 and Lsp1 exhibited low amino acid identities and similarities (Supplemental Figure S2). This is expected because a low degree of

amino acid conservation is typical among members of the BAR domain superfamily (Masuda and Mochizuki, 2010). The crystal structures of *Drosophila* amphiphysin and the C-terminal domain of human arfaptin 2 provide well-known examples of this feature: despite very low pairwise sequence identities (<14%) these BAR domain-containing proteins exhibit high structural similarity (Peter *et al.*, 2004). BAR domain-containing proteins bind and tubulate liposomes in vitro (Takei *et al.*, 1999; Peter *et al.*, 2004). To test the significance of our bioinformatics results, we performed liposome cosedimentation assays using purified full-length recombinant Pil1 and Lsp1. We observed that both proteins were able to bind liposomes (Figure 2A and Supplemental Figure S3). To test tubulation, we incubated the purified proteins with liposomes and examined their morphology by electron microscopy. Unlike the liposomes-only control, incubation with both Pil1 and Lsp1 resulted in deformed liposomes that exhibited tubules with similar diameter ( $52 \pm 7$  and  $62 \pm 9$  nm, respectively; Figure 2B and Supplemental Figure S3). We also observed that Pil1 formed filaments, suggesting that they act as linear scaffolds for liposome tubulation (Figure 2 and Supplemental Figure S3). Thus, like other BAR domain-containing proteins, Pil1 and Lsp1 are capable of binding lipids and introducing membrane curvature in vitro.

Another functional feature of BAR domain-containing proteins is their capacity to form membrane-associated tubular structures when overexpressed in mammalian cells (Lee *et al.*, 2002). To test whether Pil1 and Lsp1 induce the formation of tubular structures, untagged versions of Pil1 and Lsp1 were expressed from a strong human cytomegalovirus promoter in COS-7 cells. Given the high degree of conservation between Pil1 and Lsp1 (74% amino acid identity), both proteins can be monitored by immunofluorescence using the same polyclonal antibody. When overexpressed in COS-7 cells, Pil1 formed rod-like clusters 2–3  $\mu\text{m}$  in length (short tubes) and also dot-like clusters (Figure 3, top). The level of cytoplasmic Pil1 was found to be either very low or not detectable. Moreover, orthogonal (z, x) views of transfected cells revealed that Pil1 clusters were associated with the cell periphery (Supplemental Figure S4). Unlike Pil1, Lsp1 overexpression led to a heterogeneous population of cells exhibiting both abundant diffuse cytoplasmic material and long tubular clusters 6–7  $\mu\text{m}$  in length (Figure 3, middle). These results indicate that both Pil1 and Lsp1 are able to form tubular structures when overexpressed in a heterologous system such as COS-7 cells. Moreover, coexpression of Pil1 and Lsp1 led to a dramatic increase in the number of cells having long tubular structures, suggesting that these two proteins act cooperatively to form tubules (Figure 3, bottom). Overall, our in vitro and in vivo results indicate that Pil1 and Lsp1 are bona fide BAR domain-containing proteins.

### Positive charges of Pil1 BAR domain are important for lipid binding and tubulation

We built structural models of Pil1 and Lsp1 to further investigate the domain identity of the eisosome core. We used the program Modeller (Marti-Renom *et al.*, 2000), using five BAR domain crystal structures as templates: *Drosophila melanogaster* amphiphysin (1uru) and the human proteins sorting nexin 9 (2raj), APPL1 (adaptor protein containing pleckstrin homology [PH] domain, PTB domain, and leucine zipper motif 1) (2q13), Bin1 (2fic), and Arfaptin 2 (1i49). This selection of templates included those hits that showed the highest HHpred and COMPASS scores and more than 50% coverage of Pil1/Lsp1 amino acid sequences.

The structural models show features of the canonical topology of BAR domains: monomers with three long  $\alpha$ -helices arranged into a twisted coiled-coil defining a six-helix bundle dimer (Figure 4, A and

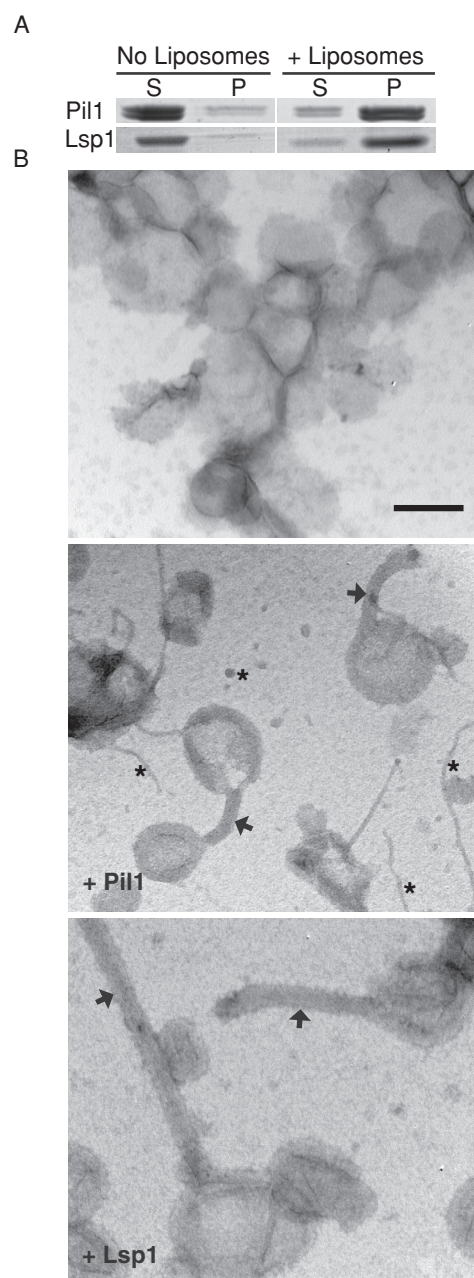


**FIGURE 2:** Pil1 and Lsp1 bind and tubulate liposomes in vitro. (A) Purified recombinant Pil1 and Lsp1 were incubated with or without bovine brain total lipid extract/PI(4,5)P2 liposomes, ultracentrifuged, and supernatant (S) vs. pellet (P) fractions were separated by SDS-PAGE and stained with Coomassie. (B) Representative electron micrographs of liposomes incubated with either Pil1 or Lsp1. Scale bar, 200 nm. Arrows and asterisks indicate liposome tubules and protein filaments, respectively.

B). Unlike amphiphysin, Pil1 and Lsp1 lack a predicted N-terminal amphipathic helix, and therefore we consider these to be classical BAR domain proteins. The structural models enabled us to identify amino acids that were potentially relevant for Pil1 and Lsp1 function. Indeed, we found a group of highly conserved residues that were structurally equivalent to residues important for amphiphysin function. Specifically, Pil1/Lsp1 Arg-145 and Lys-148 in the  $\alpha 2$  helix and Lys-159 and Lys-165 in the distal extended loop between helices  $\alpha 2$  and  $\alpha 3$  would result in positively charged surface patches on the



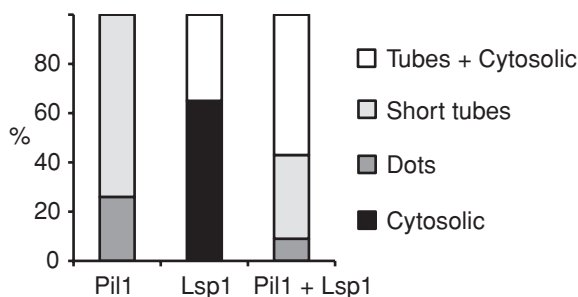
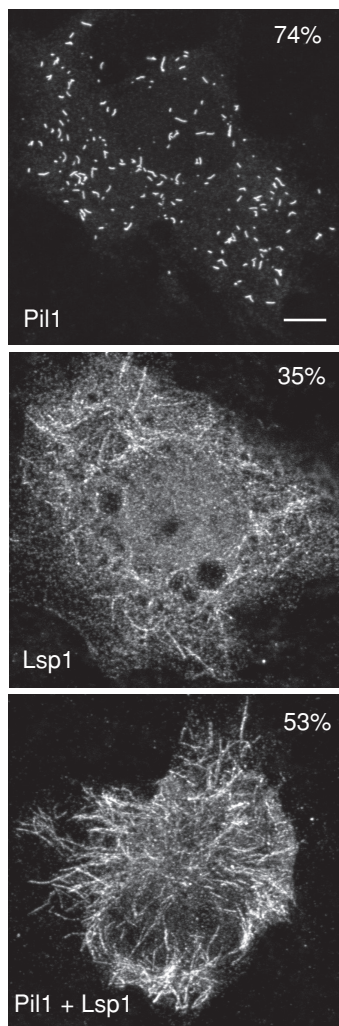


**FIGURE 3:** Pil1 and Lsp1 form tubular structures in vivo. Confocal immunofluorescence micrographs of COS-7 cells overexpressing untagged Pil1, Lsp1, or both proteins. Percentages indicate the proportion of positively transfected cells that exhibited the described pattern. Scale bar, 6  $\mu$ m. Bottom, quantitative analysis of the different distribution patterns of the proteins observed microscopically. More than 75 cells from three independent experiments were analyzed for each condition tested.

concave face of the dimer (Figure 4B). In amphiphysin, equivalent patches were shown to be necessary for binding to and bending of negatively charged membranes (Peter *et al.*, 2004). Further support for the functional importance of these residues was provided by the strict conservation within Pil1 (and Lsp1) homologues (Supplemental Figure S5). Because Pil1, but not Lsp1, is necessary for eisosome

assembly, we targeted conserved Pil1 residues. Thus we replaced Arg-145, Lys-148, Lys-159, and Lys-165 with glutamic acid residues to generate different Pil1 variants that were subsequently examined by cosedimentation assays and fluorescence microscopy. As shown in Figure 4B, all targeted residues are surface exposed. Thus substitutions in these residues would not be expected to alter the overall BAR domain structure (Peter *et al.*, 2004). As in amphiphysin, a double mutant (mut2) reduced the binding to liposomes, and the quadruple mutant (mut3) was more effective (Figure 4C). Remarkably, neither mut2 nor mut3 was able to tubulate liposomes, indicating that the targeted residues are crucial for membrane bending in vitro (Supplemental Figure S5). In addition, mut3 overexpressed in COS-7 cells had a cytoplasmic distribution, establishing that it is unable to promote formation of either dot-shaped clusters or tubular structures (Figure 4D). Thus Pil1 function is dependent on canonical BAR domain residues.

### Loss of Pil1 BAR domain positively charged residues alters eisosome biogenesis and plasma membrane organization

Given that Pil1 controls eisosome biogenesis and plasma membrane organization, we asked whether the integrity of Pil1 BAR domain was required for these functions. We introduced BAR domain variants in the context of the *PIL1-GFP* fusion gene into yeast strains as the sole source of *PIL1*. When analyzed by confocal fluorescence microscopy, the single mutant Pil1-R145E showed defects in eisosome organization (Figure 5). This phenotype was also evident for both the extended-loop K159E K165E (mut1) and the helix  $\alpha$ 2 R145E K148E (mut2) Pil1-GFP variants. In all cases fluorescence remained highly cytoplasmic, with only a few large eisosomes formed at the cell periphery (Figure 5). Similar to the phenotype exhibited by mut3 in COS-7 cells (Figure 4C), when the extended-loop and concave-surface double mutants were combined, virtually all yeast cells lacked eisosomes with mut3, being located almost exclusively in the cytoplasm (Figure 5, bottom).

Next, we tested whether other eisosomal proteins as well as MCC markers were affected. We monitored Cherry-tagged wild-type versions of Lsp1 and the integral membrane protein Sur7 in the context of GFP-tagged mut2 as the sole source of Pil1. Indeed, in mut2 *pil1* $\Delta$  cells, Lsp1 remained highly cytoplasmic, lost its regular plasma membrane pattern, and colocalized with mut2 (Figure 6A). Similarly, Sur7 dispersed homogeneously in the plasma membrane to form foci that colocalized with mut2 eisosomes (Figure 6B). Taken together, these results indicate that Pil1 BAR domain-positive patches are needed for both normal eisosome structure and plasma membrane domain organization.

To gain mechanistic insight, we further characterized the mut2 Pil1 variant. Whereas total protein levels were comparable between wild-type and mut2 Pil1, the number of eisosomes formed by mut2 was decreased threefold (Figure 7, A–C). We observed that mut2 eisosomes were larger and more heterogeneous than wild-type eisosomes (Figure 7D). We also observed that despite forming larger eisosomes, the overall proportion of plasma membrane-associated mut2 was five times lower than that of wild-type Pil1 (Figure 7E). These data suggest that mut2 is as stable as wild-type Pil1 but is defective in eisosome biogenesis. Eisosomes are formed de novo by gradual deposition of Pil1/Lsp1 on the plasma membrane of a nascent cell (Moreira *et al.*, 2009). Once formed, eisosomes were shown to be stable, having minimal exchange of assembled Pil1 subunits with the cytoplasmic pool (Walther *et al.*, 2006). Because mut2 associated poorly with the plasma membrane and remained mostly cytoplasmic, we asked whether mut2 incorporation into growing eisosomes was defective. To address this question, we measured

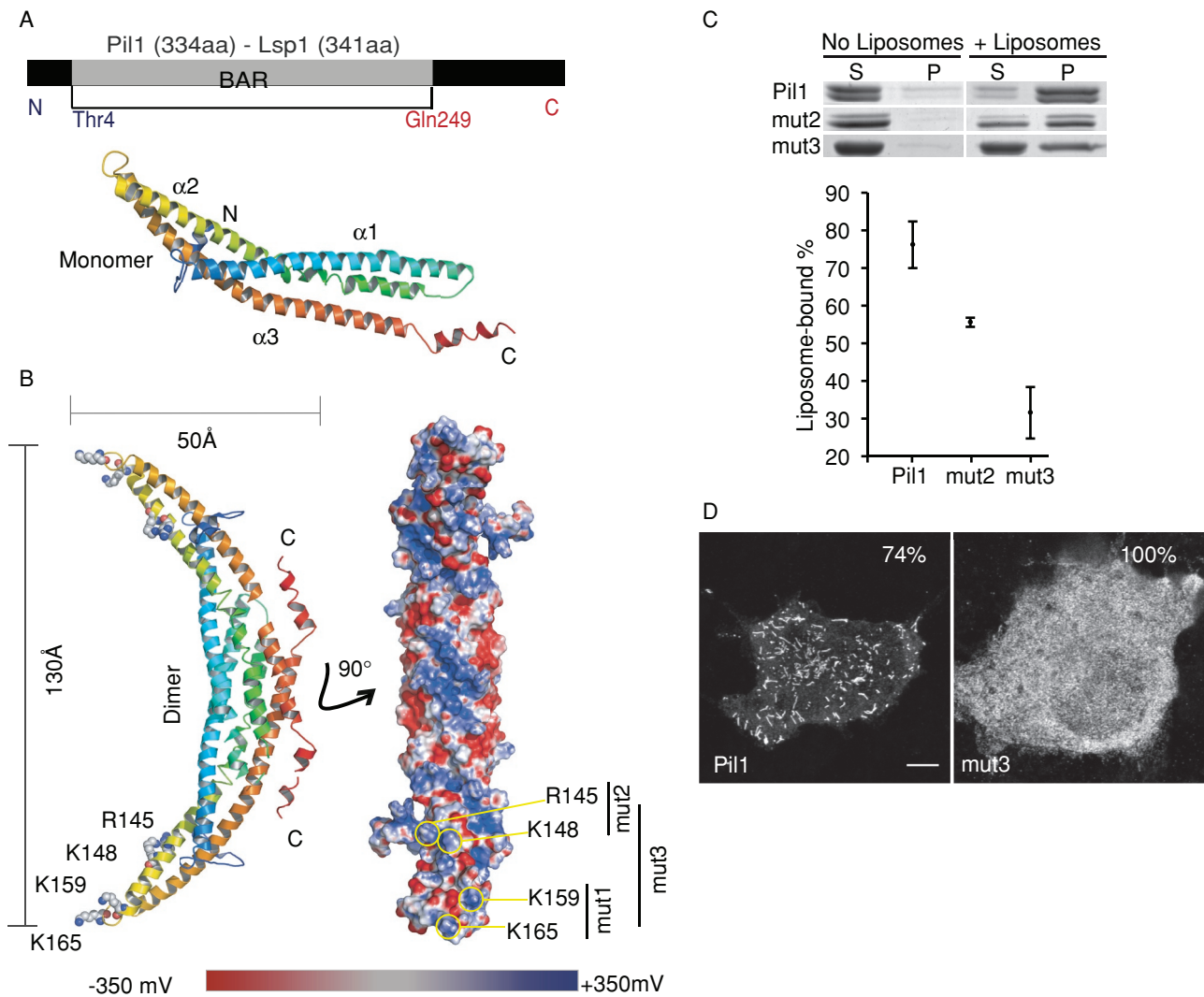


**FIGURE 4:** Structural modeling and functional analysis of Pil1 BAR domain. (A) Cartoon representation and homology model of a Pil1 monomer based on the crystal structures of five distant homologues. The chain is color coded from blue to red from N-terminus to C-terminus, respectively. Alpha helices are labeled. (B) Dimeric arrangement of Pil1. The modeled monomer was sequentially superimposed onto chains A and B of the *Drosophila* amphiphysin dimer (1URU). Cartoon representation (left) is rotated axially 90°, showing the electrostatic surface of the concave side of the dimer (right). Conserved basic residues that were targeted for mutagenesis studies are indicated. (C) Purified recombinant wild-type, mut2, and mut3 versions of Pil1 were tested for binding to liposomes. Quantification of two independent experiments is in the graph below; error bars correspond to standard deviations. (D) Confocal immunofluorescence micrographs of COS-7 cells overexpressing wild-type or mut3 Pil1. Percentages indicate the proportion of cells that exhibited the pattern shown. Scale bar, 6  $\mu$ m.

the formation rate of individual eisosomes in yeast cells expressing Pil1–green fluorescent protein (GFP). As we previously reported, Pil1 assembly was characterized by a period of rapid incorporation followed by a plateau (Figure 8A, left). Compared with wild type, mut2 was incorporated at a similar rate but without reaching a discernible plateau (Figure 8A, right). Prolonged assembly of mut2 was consistent with large eisosomes formed by this mutant but did not explain why it remained highly cytoplasmic (Figure 7). One possibility is that mut2 eisosomes are abnormally unstable, and therefore assembled mut2 subunits exchange at high rates with the cytoplasmic pool. To test whether mut2 eisosomes were unstable, we performed fluorescence recovery after photobleaching (FRAP) analysis of GFP-tagged wild-type and mut2 Pil1. Over a 45-min time period after eisosome bleaching, wild-type and mut2 Pil1-GFP fluorescence recovered with similar kinetics, indicating that mut2 eisosomes were as stable as

wild type (Figure 8B). Therefore it is unlikely that eisosome instability causes the observed high levels of cytoplasmic mut2. An alternative explanation for this phenotype is that in mut2 *pil1* $\Delta$  cells fewer sites become effective for eisosome assembly (Figure 7C). Given that mut2 protein levels (Figure 7B), assembly rate (Figure 8A), and eisosome stability (Figure 8B) were normal, a limited number of effective nucleation sites should cause a surplus of cytoplasmic mut2. Thus mut2 main defect may be due to failure in nucleation site formation. If correct, introduction of wild-type Pil1 in mut2 *pil1* $\Delta$  cells should restore the number of effective nucleation sites, leading to incorporation of mut2 into eisosomes of normal size. When Pil1-Cherry was introduced into mut2 cells, normal eisosome number and size were restored (Figure 8C). Thus we conclude that the conserved positive patch of the Pil1 concave face is important for generation of eisosome nucleation sites at the plasma membrane.

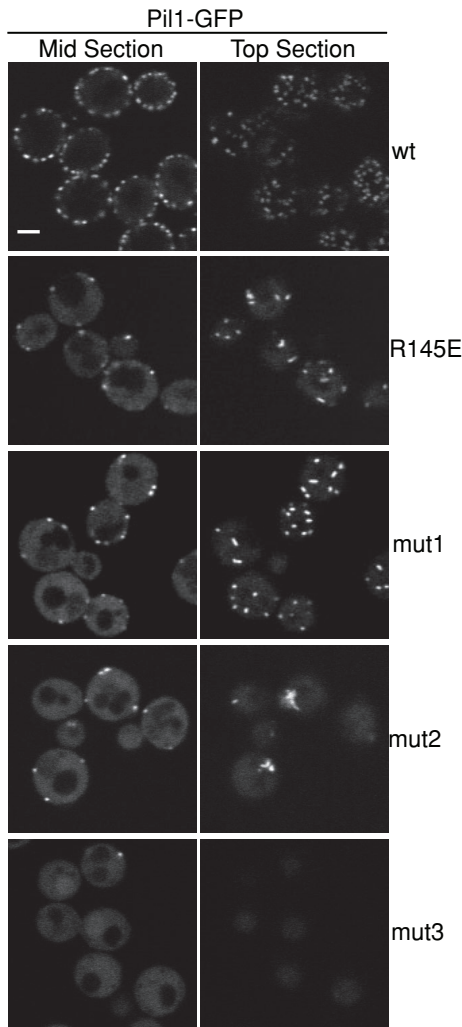


**FIGURE 5:** Pil1 BAR domain positively charged residues are necessary for eisosome assembly and organization. The C-terminally GFP-tagged versions of wild-type (wt), mut1, mut2, or mut3 Pil1 were expressed under control of the endogenous promoter in *pil1Δ* yeast cells. Representative confocal micrographs of mid and top sections are shown. Scale bar, 2  $\mu$ m.

#### F-BAR PH domains of Slm1 and Slm2 are sufficient for recruitment to eisosomes

Slm1 and Slm2 form an essential protein pair that promotes actin cytoskeleton organization, sphingolipid homeostasis, and cell growth (Audhya *et al.*, 2004; Tabuchi *et al.*, 2006). Fluorescently tagged Slms were visualized as plasma membrane foci that colocalized with eisosomes (Grossmann *et al.*, 2008). Slms mutants lacking PH domains associate poorly with the plasma membrane but are still able to form foci (Audhya *et al.*, 2004; Fadri *et al.*, 2005). Moreover, GFP fused to the PH domain of either Slm1 or Slm2 PH is homogeneously distributed along the plasma membrane, with no distinguishable foci (Yu *et al.*, 2004). These reports indicated that Slms PH domains are sufficient for plasma membrane binding but not for recruitment to eisosomes. Because our bioinformatics results suggested that Slm proteins have F-BAR domains, we tested whether these domains were important for Slms targeting to eisosomes. We generated GFP N-terminally tagged versions of each Slm F-BAR and F-BAR-PH domains and then analyzed their localization in the context of cells expressing Pil1-Cherry. We found that both F-BAR

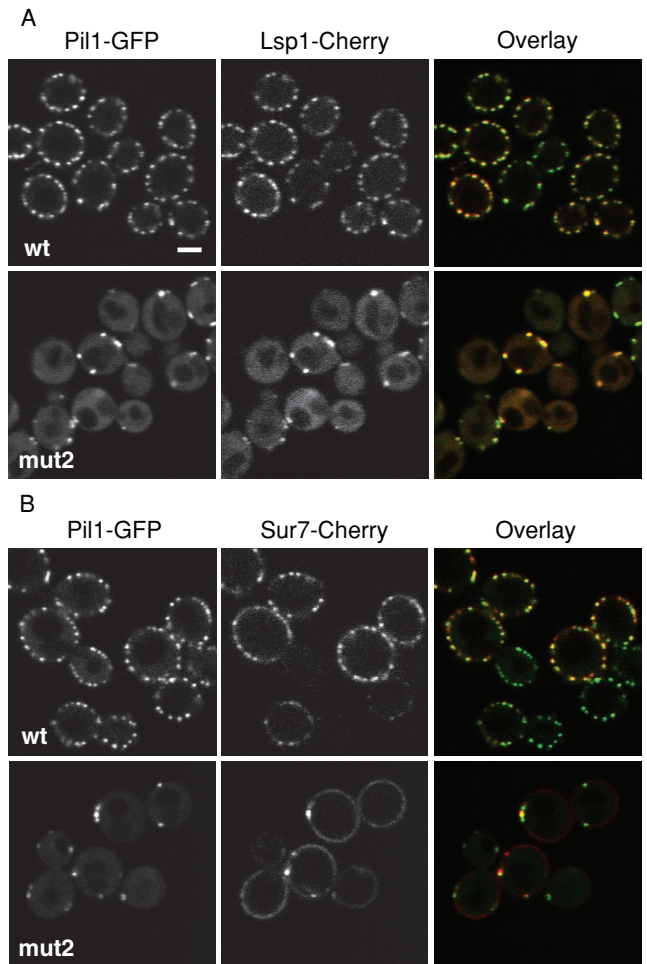


**FIGURE 6:** MCC organization is disrupted in Pil1 BAR domain mutants. Representative confocal midsection micrographs of Lsp1-Cherry (A) and Sur7-Cherry (B) cells expressing wild-type (wt) and BAR domain mutant variants of Pil1-GFP. Scale bar, 2  $\mu$ m.

domains disperse in the cytoplasm and also form foci that are not associated with the plasma membrane (Figure 9). However, when we tested fusions that contained both the F-BAR and the PH domains we found that they colocalized with Pil1-Cherry. These results indicate that the F-BAR and the PH domains collaborate to target Slm proteins to eisosomes.

#### DISCUSSION

Here we describe how a substantial fraction of eisosome proteins have domains predicted to engage in protein–protein and protein–lipid interactions. The core components of eisosomes, Pil1 and Lsp1, are BAR proteins. Pil1 BAR domain integrity is crucial for both eisosome assembly and plasma membrane domain organization. In addition, TORC2 substrates Slm1 and Slm2 have F-BAR domains that are needed for targeting into eisosomes.

#### Pil1/Lsp1 BAR domains and eisosome biogenesis

Our study establishes that Pil1 and Lsp1 are BAR domain-containing proteins. Cryo–electron microscopy data show that BAR domain-containing proteins form coats on membrane surfaces and introduce changes in their curvature (Frost *et al.*, 2009). Thus eisosomes may be arranged as bidimensional lattices that structure the yeast plasma membrane into furrow-like invaginations. Eisosome



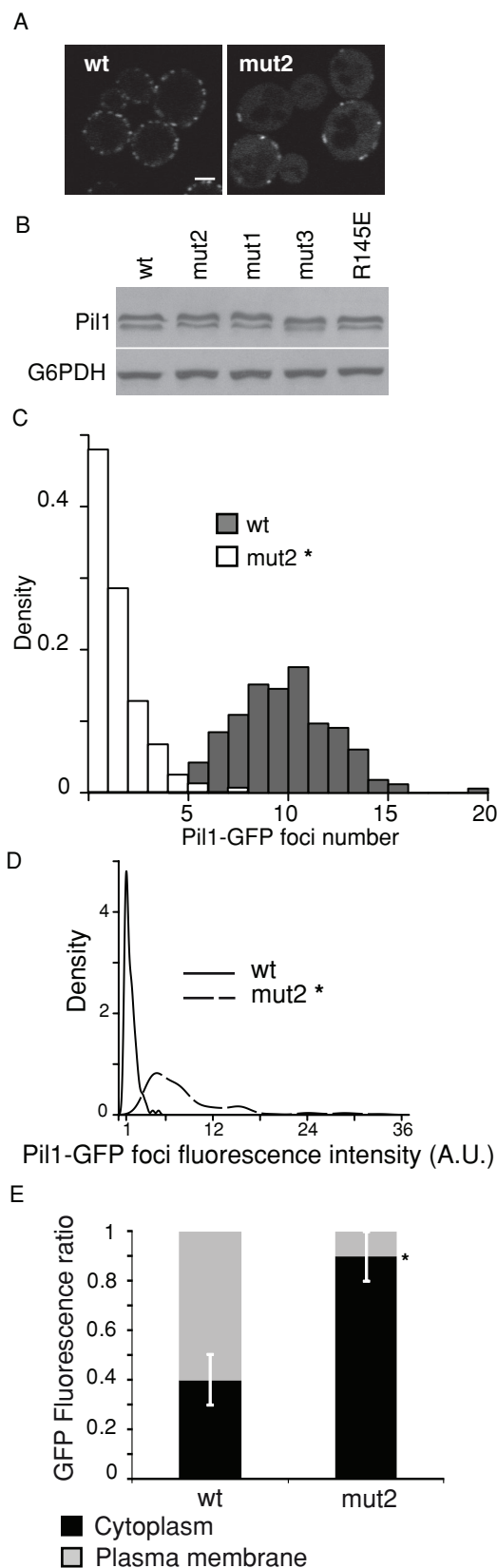


**FIGURE 7:** Mut2 Pil1 is defective in plasma membrane association and forms abnormally large assemblies. *pil1* $\Delta$  yeast cells expressing C-terminally GFP-tagged wild-type (wt) or mut2 Pil1 were grown in SC media at 30°C to mid-log phase and then imaged using the same microscope settings. Fluorescence measurements were made for a total of 150 yeast mother cells with small and medium-sized buds as

biogenesis can be divided into three main stages: nucleation site formation, active assembly, and completion of assembly (Moreira *et al.*, 2009). Eisosome random distribution indicates that nucleation sites are generated by stochastic events (Moreira *et al.*, 2009). We postulate that these stochastic events depend on direct binding of Pil1 to the plasma membrane. In this scenario, cytoplasmic Pil1 dimers (or low-order preassembled oligomers) collide with the newly formed plasma membrane and bind to negatively charged lipids involving BAR domain-mediated electrostatic interactions. Thus the formation of nucleation sites should be modulated by Pil1 cytoplasmic levels (number of collision events) and by lipid-protein interaction strength (stability of the nucleation site formed). Consistent with this hypothesis, the number of eisosomes per cell surface area is directly proportional to Pil1 availability: a surplus of Pil1 leads to an increase in eisosome surface density, and conversely, a shortage of Pil1 results in a decrease in eisosome density (Moreira *et al.*, 2009). The observed phenotypes for mut2 and mut3 Pil1 variants, which have reduced lipid-binding capacity, are also consistent with this hypothesis (Figures 4, 5, 7, and 8 and Supplemental Figure S6). Our analysis of mut2 eisosomes biogenesis and stability also agrees with the presence of defects in nucleation site formation (Figure 8).

Pil1 and Lsp1 are phosphorylated by the eisosome-associated kinases Pkh1 and Pkh2 (Zhang *et al.*, 2004; Walther *et al.*, 2007; Luo *et al.*, 2008). Perturbation of Pil1 phosphorylation status affects eisosome assembly, but how assembly is affected is still debated (Walther *et al.*, 2007; Luo *et al.*, 2008). Of interest, structural modeling analysis indicates that many phosphorylated Pil1 residues (Ser-26, Thr-28, Ser-41, Ser-45, Ser-59, and Ser-163) lie in the concave face of the BAR domain (Supplemental Figure S7 and additional supplementary material). Further studies dissecting the role of specific Pil1/Lsp1 residues on membrane binding and assembly should clarify this issue. It is highly likely that eisosome biogenesis involves other factors. Indeed, recent analysis of eisosome protein Ymr086w (FEA1) indicated that it regulates eisosomes biogenesis, either by stabilizing formation of nucleation sites or promoting bidimensional assembly (Peter Walter, personal communication).

#### Eisosome core proteins and BAR domain-dependent plasma membrane organization

Through this study eisosome-mediated membrane bending emerges as the driving force for MCC domain organization. Curvature-induced lipid segregation has been theoretically described and experimentally demonstrated (Markin, 1981; Roux *et al.*, 2005). Thus Pil1/Lsp1-mediated initial membrane bending may induce lipid segregation and thereby facilitate the recruitment of proteins and lipids required for both eisosome building and MCC maturation. This mechanism may be sustained by a positive-feedback cycle for protein/lipid recruitment and curvature propagation that eventually is shut down by Pil1 depletion. We do not know whether Pil1 and Lsp1 are sufficient to build and organize MCCs. In vitro reconstitution of MCC formation using synthetic lipids and purified proteins would be an important step in

part of three independent experiments. (A) Representative mid section confocal micrographs. Scale bar, 2  $\mu$ m. (B) Western blot analysis of Pil1-GFP mutants. G6PDH is shown as a loading control. (C) Density distribution of Pil1-GFP foci number in mid confocal sections. (D) Density distribution of fluorescence intensities of GFP foci. (E) Cytoplasmic and plasma membrane-associated GFP fluorescence ratios. Error bars correspond to standard deviations. \* $p < 0.05$ .



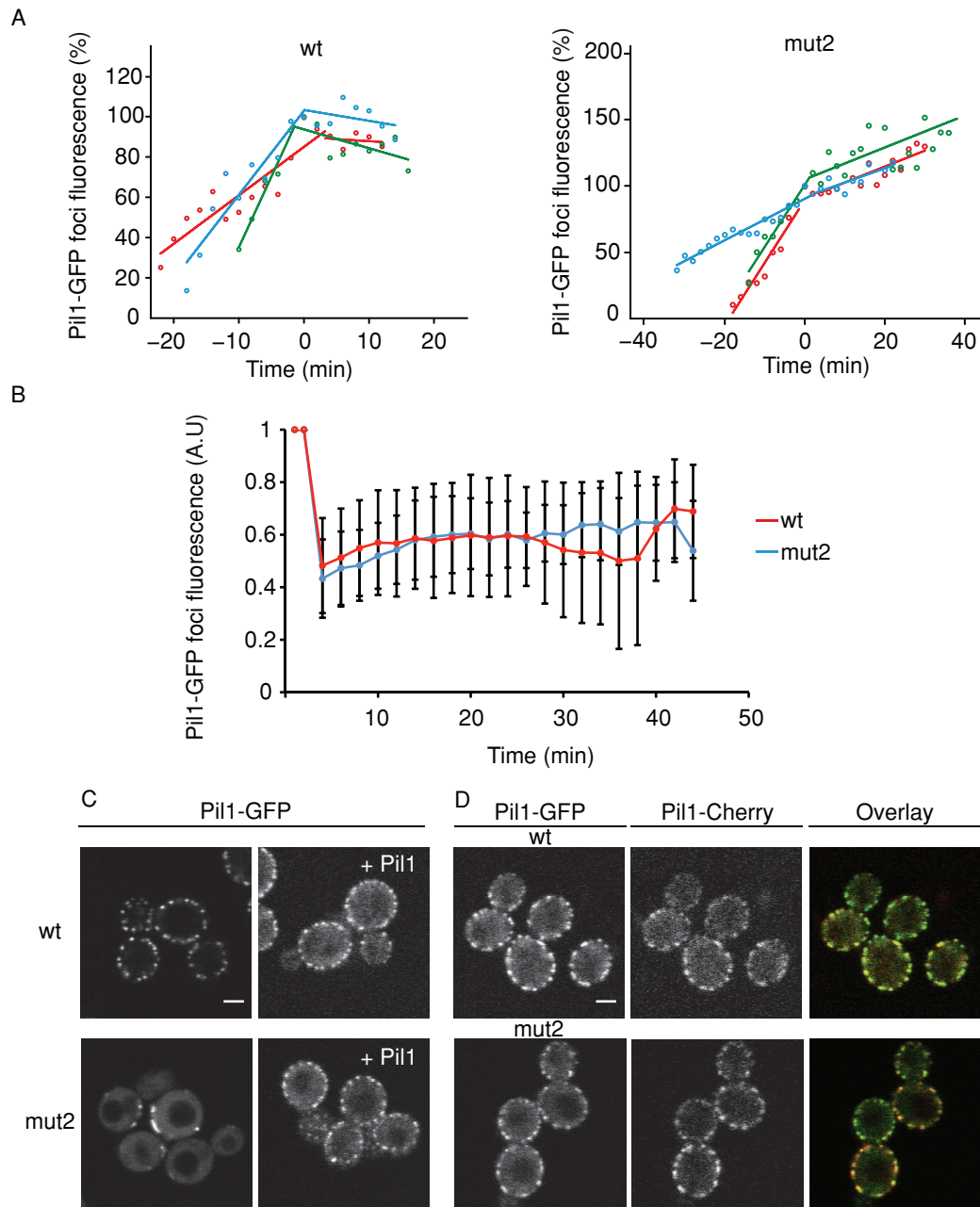


**FIGURE 8:** Mut2 Pil1 is defective in nucleation site formation. Yeast strains were grown in SC at 30°C to mid-log phase and then imaged by confocal 3D time-lapse microscopy under the same growth conditions. (A) Mut2 assembly rate is normal but prolonged. Measurement of fluorescence intensity of individual Pil1 foci in growing buds. Three representative examples are shown for each strain. Each data set was fit to a bilinear behavior using the Davies test. The point where a change in the slope was detected was defined as time 0 and 100% of relative fluorescence units. Negative slopes observed for wild-type Pil1-GFP fluorescence at late time points are likely due to inefficient bleaching correction (see *Materials and Methods* for details). (B) Mut2 eisosomes are as stable as wild type. Pil1 foci were bleached (time = 0), and fluorescence recovery was monitored over time. Fluorescence measurements were made for a total of 25 bleached foci as part of three independent experiments. Error bars indicate standard deviations. (C, D) Wild-type Pil1 complements mut2. Representative confocal micrographs of mid sections of yeast cells expressing fluorescently tagged versions of Pil1 are shown. (C) GFP-tagged wild-type and mut2 Pil1 cells with (right) and without (left) the wild-type *PIL1* gene under control of its own promoter. (D) GFP-tagged wild-type and mut2 Pil1 cells with an extra copy of wild-type *PIL1-mCherry* under control of *PIL1* native promoter. Scale bars, 2  $\mu$ m.

determining the minimal machinery required for eisosome-driven membrane compartmentalization.

There is a remarkable difference between Pil1/Lsp1 and currently described BAR domain-containing proteins: rather than being directly involved in transient changes of membrane structure, Pil1 and

Lsp1 mediate a permanent membrane remodeling event. *S. cerevisiae* BAR domain-containing proteins Rvs161/Rvs167 and Syp1 participate dynamically in different stages of clathrin/actin-mediated endocytosis (Stimpson *et al.*, 2009; Youn *et al.*, 2010). The role of eisosomes in yeast endocytosis is a matter of debate (Walther *et al.*,

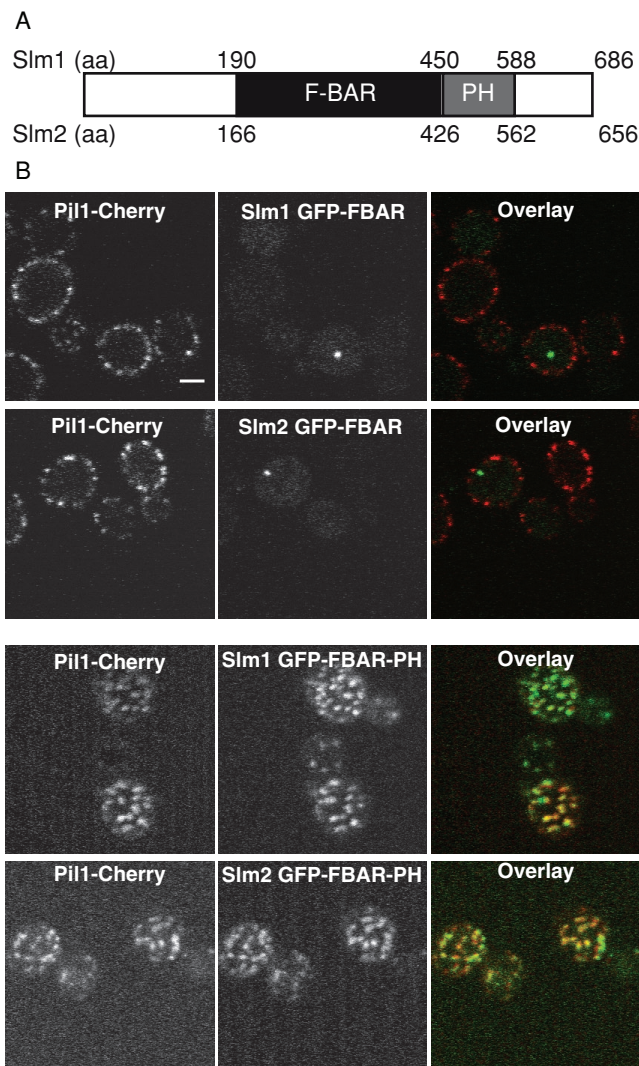


**FIGURE 9:** Slms F-BAR domains are required for targeting to eisosomes. (A) Cartoon representation of Slm1 and Slm2 domains analyzed in this work. (B) Representative confocal mid section micrographs of Pil1-Cherry cells expressing N-terminally tagged Slm1 and Slm2 F-BAR (top) and F-BAR-PH (bottom) domains. Scale bar, 2  $\mu$ m.

2006; Grossmann *et al.*, 2008). Our FRAP analysis showed that eisosomes are not as stable as we reported previously (Walther *et al.*, 2006). The reason for this discrepancy might be that here we monitored fluorescence recovery over a period five times longer, comparable to the length of half the cell cycle. This turnover of Pil1 may be evidence of normal maintenance of the Pil1/Lsp1 coat that holds the furrow-like invaginations. In addition, the turnover could reflect a highly dynamic subpopulation of Pil1 that, like other BAR domain-containing proteins, may be directly implicated in endocytic events.

### Recruitment of Slms to the plasma membrane

Our bioinformatics results indicated that the so-called “Slm domains” are likely to be F-BAR domains. We have shown that these domains, in conjunction with their cognate PH domains, were sufficient for targeting to eisosomes (Figure 9). Work from the Emr and Hall groups described different temperature-sensitive Slm1 mutant alleles lacking plasma membrane localization (Audhya

*et al.*, 2004). Of interest, many mutations found in these alleles involved basic residues of its putative F-BAR domain. Isolated Slms PH domains distributed GFP homogeneously at the plasma membrane (Yu *et al.*, 2004). Thus Slms PH domains may confer a broad specificity for the plasma membrane, whereas the F-BAR domains refine this specificity to eisosome-associated plasma membrane domains (MCCs). What do F-BAR PH Slms domains interact with in MCCs? It is possible that an unidentified protein mediates Slms recruitment. However, since PH and BAR domains bind negatively charged lipids, it seems more likely that Slms targeting is mediated by protein–lipid interactions. In vitro binding assays showed that Slms PH domains have very low phosphoinositide-binding specificity (Yu *et al.*, 2004). Several F-BAR domains preferentially bind phosphatidylserine and phosphoinositides (Itoh *et al.*, 2005). Thus it is possible that Slms F-BAR PH domains have a characteristic phosphoinositide-binding preference that is specific for MCCs. As such, it will be of interest to test the membrane-binding preferences of Slms PH domains with and without their cognate F-BAR domains. Another possibility is that Slms F-BAR PH domains sense two MCC features: lipid composition and curvature. Cryo–electron microscopy studies of membrane-bound BAR domain-containing proteins coats showed the existence of periodic discontinuities that leave enough room for access of other proteins to the lipid leaflet (Frost *et al.*, 2008). Thus Slm proteins may interact with the plasma membrane furrow-like invaginations percolating a Pil1-Lsp1 coat.

Slms are TORC2 effectors, they physically interact with TORC2 protein Avo2, and both are phosphorylated in vitro by TORC2 (Audhya *et al.*, 2004). An apparent paradox with this physical link between Slms and TORC2 is that the expected localization for Slms are MCTs, whereas they were found to be localized to eisosomes. Live microscopy data monitoring Slms in the context of TORC2 and eisosomes will help to resolve this issue. It is proposed that, by integrating information from different plasma membrane domains, Slm proteins regulate actin cytoskeleton dynamics, cell growth, and sphingolipid metabolism (Aronova *et al.*, 2008; Berchtold and Walther, 2009). Further characterization and manipulation of domain-specific Slms targeting cues will facilitate analysis of these intricate signaling networks.

## MATERIALS AND METHODS

### Growth conditions, yeast strains, and plasmids

Unless otherwise indicated, yeast cells were grown at 30°C in synthetic complete (SC) media. All yeast strains used are listed in Supplemental Table S1. Gene replacements were done by homologous recombination using a standard PCR-based method (Longtine *et al.*, 1998). Variants of pRS306-PIL1-GFP plasmid (Walther *et al.*, 2007) were obtained by site-directed mutagenesis (QuikChange; Stratagene, Santa Clara, CA). Different Slm domains were cloned into pEW331. The amino acid residues included in various constructions were based on complete open reading frame (ORF) sequences (*Saccharomyces* Genome Database [SDG], <http://www.yeastgenome.org>) and were Slm1 BAR 155–484, Slm1 BAR PH 155–588, Slm2 BAR 145–461, Slm2 BAR PH 145–570, Rgc1 BAR 136–510, and Rgc1 BAR PH 136–731. All constructions were verified by DNA sequencing.

### Bioinformatics standard and distant homologue searches

Initial searches were done using Position-Specific Iterative (PSI)-BLAST (Altschul *et al.*, 1997) against the nonredundant database. After the fourth iteration, hits with E values  $<10^{-3}$  were selected for further analysis. These selected hits were, in turn, aligned with the

halign procedure from the HHsearch package. Resulting multiple sequence alignments (MSAs) were used to scan the PDB, Pfam, and SCOP databases (Berman *et al.*, 2007; Andreeva *et al.*, 2008; Finn *et al.*, 2010), using the algorithms of HHsearch (Soding, 2005) and COMPASS (Sadreyev *et al.*, 2003). In the case of HHsearch, the CDD (Marchler-Bauer *et al.*, 2007) and SUPFAM (Pandit *et al.*, 2002) databases were also queried. Sequences generating no significant results were iteratively chopped, resubmitted (with sequentially modified BLAST parameters), and resulting MSAs were inspected and edited.

### Structural modeling

Homology model for the monomer of Pil1 was built using five different BAR/N-BAR domains as structural templates (1URU, 2RAJ, 2Q13, 2FIC, and 1149). Template crystal structures were superimposed using STAMP (Russell and Barton, 1992). Pil1 and Lsp1 sequences were aligned with this structure-based MSA using T-Coffee (Notredame *et al.*, 2000). The final MSA was used to build the homology structural model using Modeller (version 9v3). The best model obtained from 50 iterations was determined with the DOPE method, included in the Modeller suite. The overall quality of this model, including side chain and rotamer fixing and rebuilding, was verified with Coot (Emsley and Cowtan, 2004). Dimer assembly was manually built using Coot based on the crystal structure of the amphiphysin BAR domain from *D. melanogaster* as reference (1URU) (Peter *et al.*, 2004). Surface interaction between monomers in the Pil1 dimer obtained were optimized energetically with RosettaDock (Sircar *et al.*, 2010). Electrostatic calculations were made with the Adaptive Poisson–Boltzmann Solver (Baker *et al.*, 2001). All figures illustrating protein structure were prepared using PyMOL (<http://www.pymol.org/>).

### Phylogenetic reconstructions

Phylogenetic trees were inferred using phyML (Guindon and Gascuel, 2003) with JTT +G+F as protein evolution model (Jones *et al.*, 1992). The evolution model was chosen using ProtTest (Abascal *et al.*, 2005).

### Recombinant protein expression and purification

The entire coding sequences of Pil1, mut2, mut3, and Lsp1 were subcloned into the pGEX4T2 vector (GE Healthcare Biosciences, Piscataway, NJ) and expressed in *Escherichia coli* BL21D3pLys strain. For protein expression, cells were grown to OD<sub>600 nm</sub> 0.8 in 2 l of Luria–Bertani medium (supplemented with carbenicillin 100 µg/ml) at 37°C and 220 rpm. Then 1 mM isopropyl β-D-thiogalactopyranoside was added, and cells were grown another 4 h at 25°C and 220 rpm. Cells were harvested and suspended in lysis buffer (1× phosphate-buffered saline [PBS], 0.5 M NaCl, 2 mM magnesium acetate, 1 mM dithiothreitol [DTT], 400 µg/ml lysozyme, and Complete Protease Inhibitor [Roche Applied Science, Mannheim, Germany]). Cells were disrupted by sonication, and the soluble protein fraction was obtained by centrifugation (17,500 × *g*, 45 min, 4°C) and filtration (0.45-µm filter; Millipore, Billerica, MA). The soluble fraction was injected in a GStap HP (GE Healthcare), and on-column digestion with 5 U/mg of thrombin was performed overnight at 22°C. A second purification step was performed using a Resource-Q ionic interchange column (GE Healthcare). Protein was eluted using 1× PBS with a linear gradient of 1 M NaCl from 1 to 100% and then stored at 4°C. Protein integrity and identity were analyzed by a SDS–PAGE electrophoresis, followed by mass spectrometry.

### Liposome preparation, liposome binding, and in vitro tubulation assays

Lipids were combined in mixtures composed of (85/15 mass %) bovine brain total lipid extract/PI(4,5)P2 (Avanti Polar Lipids, Alabaster, AL), dissolved in chloroform/methanol (2/1 vol %), dried under a stream of argon in glass vials, and desiccated under high-vacuum for 1 h. Lipids were then hydrated with 2 mM DTT in 1× PBS buffer, gently vortexed, subjected to four freeze–thaw cycles, and immediately extruded using 100-nm filters. Homogeneity of liposome preparations was tested using dynamic light scattering. For liposome binding assays, proteins were precentrifuged at 100,000 × *g* for 15 min at 4°C. Protein supernatants were quantified, diluted to 1.6 µM, and incubated with liposomes (1.9 µg/µl) in 1.6 mM DTT 1× PBS buffer for 10 min at room temperature. Protein–liposome mixtures were then centrifuged at 100,000 × *g* for 15 min at 4°C. Supernatant versus pellet fractions were separated by SDS–PAGE and stained with Coomassie. Images of the Coomassie-stained gels were captured using an ImageScanner (GE Healthcare) and analyzed with tool “gels” from ImageJ software (National Institutes of Health, Bethesda, MD). Liposome-bound values were determined as the pellet percentage in the presence of liposomes subtracted by the same percentage without liposomes.

For tubulation assays, liposomes (1.2 µg/µl) were incubated with recombinant protein (25 µM) for 10 min at room temperature. Samples were loaded on carbon-coated copper grids, negatively stained using 1% uranyl acetate for 2 min at room temperature, and imaged using a JEOL (Peabody, MA) JEM 1010 electron microscope operated at 80 kV.

### Fluorescence microscopy

For fluorescence microscopy, yeast cells were grown to mid-log phase in SC medium at 30°C. Cells were mounted in the same media on glass-bottom microplates previously coated with concanavalin A and directly imaged with a Leica TCS SP5 confocal microscope at 30°C. For quantitative analyses of mut2 distribution, fluorescence images to be compared were taken using the same microscope settings. Images were analyzed using ImageJ software. Three independent experiments were done for each analysis, and 50 cells per experiment were analyzed. Stack-by-stack region-of-interest (ROI) subtraction was used for background correction. Because eisosomes are formed *de novo* in daughter cells, only mother cells were analyzed. For eisosome foci analysis a segmentation procedure was used using the manual threshold tool of ImageJ software (with the same parameters used for all of the images of each strain analyzed). Plasma membrane-associated fluorescence of each cell was calculated as the sum of fluorescence of all foci. Then cytoplasm fluorescence was calculated as the subtraction of plasma membrane fluorescence from total fluorescence. Statistical analysis was done using nonparametric tests (Mann and Whitney, 1947).

To measure eisosome formation rate, time-lapse movies were convolved (Huygens Essential, version 3.5) and further analyzed. Individual eisosomes were identified and manually tracked over time. For each time point, Z-sum projections of three stacks encompassing the whole eisosome were used to calculate the integrated fluorescence density. For bleaching correction, total fluorescence of mother cells was recorded over time. Nonimaged mother cells did not undergo detectable changes in Pil1–GFP fluorescence during the time course of the experiment (80 min). Thus we assumed that in time-lapse movies the decay in fluorescence exhibited by mother cells was due to photobleaching. A bleaching correction factor *C* was independently calculated for each movie:  $C = \frac{ID_i}{ID(t)}$ , where *ID<sub>i</sub>* is the averaged whole-mother-cell integrated fluorescence density at



time 0 and  $ID(t)$  is the density at a given time. Each data set was analyzed using the package Segmented (<http://cran.r-project.org>). First, the Davies test (Davies, 1987) was applied to evaluate whether each data set adjusted to a linear model with either a single break point (two lines) or no break point (one line). For all cases a single break point was detected with a  $p$  value of 0.05. Then segmented regression analysis was applied to determine the pair of slopes found for each data set.

For FRAP experiments cells were first imaged over six Z-stacks using a pinhole of 2 Airy units. ROIs were then bleached with 10 high-intensity laser pulses, and postbleach images were acquired every 2 min using the same settings as in prebleach scanning. Image analysis was done using the double normalization method (Phair *et al.*, 2004). Briefly, average prebleach whole-mother-cell intensity ( $I_{\text{whole-pre}}$ ) divided by the normalized whole-mother-cell intensity at each time point in the postbleach period [ $I_{\text{whole-pre}}(t) - I_{\text{base}}(t)$ ] was multiplied by FRAP-normalized ROI intensities at that time point ( $\frac{I_{\text{ROI}}(t) - I_{\text{base}}(t)}{I_{\text{ROI-pre}}}$ ). Thus, for each time point the double-normalized FRAP values [ $I_{\text{ROI-dn}}(t)$ ] were calculated using the following expression:

$$IP_{\text{UP-ROI-dn}}(t) = \frac{I_{\text{ROI}}(t) - I_{\text{base}}(t)}{I_{\text{ROI-pre}}} \times \frac{I_{\text{whole-pre}}}{I_{\text{whole}}(t) - I_{\text{base}}(t)}$$

where  $I_{\text{ROI}}(t) - I_{\text{base}}(t)$  is the normalized ROI intensity at each time point,  $I_{\text{ROI-pre}}$  is the prebleach ROI intensity, and  $I_{\text{base}}(t)$  is the background intensity corresponding to each case (ROI and whole mother cell) at each time point.

### Western blots

Cells were grown under the same conditions that were used for live confocal microscopy. Cell-free crude extracts were prepared by bead-beating lysis using 8 M urea, 50 mM HEPES, pH 7.4. Protein concentration was determined by the BCA method (Sigma-Aldrich, St. Louis, MO). An amount of 10  $\mu\text{g}/\text{lane}$  of total protein extract was electrophoresed on 10% SDS-polyacrylamide gels and transferred to polyvinylidene difluoride membranes. Membranes were blocked with PBS containing 0.05% Tween 20 (PBST) and 5% nonfat milk for 1 h at room temperature and then incubated with primary antibodies overnight at 4°C. Membranes were washed with PBST, incubated with horseradish peroxidase-conjugated secondary antibody for 1 h at room temperature, and developed using an enhanced chemiluminescence kit (Amersham Biosciences, GE Healthcare Bio-Sciences, Piscataway, NJ). For Pil1 detection polyclonal anti-Pil1 antibody was used at a 1:20,000 dilution (Moreira *et al.*, 2009). Anti-glucose-6-phosphate dehydrogenase (a-G6PDH) antibody (Sigma-Aldrich) was used at a 1:10,000 dilution.

### Constructs, COS-7 cell transfection, and immunofluorescence

Pil1, Pil1 mut3, and Lsp1 genes were subcloned in pcDNA3.1+ plasmid (Invitrogen, Carlsbad, CA). Slm2 and Rgc1 BAR and BAR PH domains were cloned in plasmid pEGFP-C3 (Clontech, Mountain View, CA). The limits of constructs, in base pair number of entire ORF sequence from the SGD, are Slm2 BAR 145–461, Slm2 BAR-PH 145–570, Rgc1 BAR 136–510, and Rgc1 BAR-PH 136–731. COS-7 cells (kindly provided by Carlos Robello) were maintained in DMEM supplemented with 10% fetal bovine serum (FBS). Coverslip-cultured cells were transfected using Lipofectamine 2000 (Invitrogen). For immunocytochemistry, after 24 h of transfection, cells were fixed in 4% formaldehyde for 20 min, permeabilized with 0.1% Triton X-100 for 15 min, and immunostained with an anti-Pil1 antibody. Secondary antibodies

were conjugated with Alexa Fluor 488 or 633 (Invitrogen). The coverslips were mounted using ProLong Gold antifade reagent from Invitrogen and imaged after 24 h with a Leica TCS SP5 confocal microscope.

### ACKNOWLEDGMENTS

We thank Hugo Naya for help with statistical analysis and Javier Valdez, Paul Gill, Arlinet Kierbel, Hector Romero, and Alejandro Colman-Lerner for discussions and critical reading of the manuscript. We also thank the Recombinant Proteins Unit, Ana Denicola, and Ernesto Cuevasanta for help with proteins and liposomes and Ariel Chaparro, Ivana Faccini, and Virginia Gorrostorrazo for administrative support. This work was supported by the Agencia Nacional de Investigación e Innovación (INNOVA URUGUAY-DCI-ALA/2007/19.040 URU-UE, P.S.A.; FCE2007\_377, M.G.; Sistema Nacional de Becas, A.O.-C.; and Sistema Nacional de Investigadores, L.H., P.S.A.) and the Programa de Desarrollo de Ciencias Básicas.

### REFERENCES

- Abascal F, Zardoya R, Posada D (2005). ProtTest: selection of best-fit models of protein evolution. *Bioinformatics* 21, 2104–2105.
- Aguilar PS *et al.* (2010). A plasma-membrane E-MAP reveals links of the eisosome with sphingolipid metabolism and endosomal trafficking. *Nat Struct Mol Biol* 17, 901–908.
- Altschul SF, Madden TL, Schaffer AA, Zhang J, Zhang Z, Miller W, Lipman DJ (1997). Gapped BLAST and PSI-BLAST: a new generation of protein database search programs. *Nucleic Acids Res* 25, 3389–3402.
- Andreeva A, Howorth D, Chandonia JM, Brenner SE, Hubbard TJ, Chothia C, Murzin AG (2008). Data growth and its impact on the SCOP database: new developments. *Nucleic Acids Res* 36, D419–D425.
- Aronova S, Wedaman K, Aronov PA, Fontes K, Ramos K, Hammock BD, Powers T (2008). Regulation of ceramide biosynthesis by TOR complex 2. *Cell Metab* 7, 148–158.
- Audhya A, Loewith R, Parsons AB, Gao L, Tabuchi M, Zhou H, Boone C, Hall MN, Emr SD (2004). Genome-wide lethality screen identifies new P14,5P2 effectors that regulate the actin cytoskeleton. *EMBO J* 23, 3747–3757.
- Baker NA, Sept D, Joseph S, Holst MJ, McCammon JA (2001). Electrostatics of nanosystems: application to microtubules and the ribosome. *Proc Natl Acad Sci USA* 98, 10037–10041.
- Berchtold D, Walther TC (2009). TORC2 plasma membrane localization is essential for cell viability and restricted to a distinct domain. *Mol Biol Cell* 20, 1565–1575.
- Berman H, Henrick K, Nakamura H, Markley JL (2007). The worldwide Protein Data Bank (wwPDB): ensuring a single, uniform archive of PDB data. *Nucleic Acids Res* 35, D301–303.
- Collins SR, Kemmeren P, Zhao XC, Greenblatt JF, Spencer F, Holstege FC, Weissman JS, Krogan NJ (2007). Toward a comprehensive atlas of the physical interactome of *Saccharomyces cerevisiae*. *Mol Cell Proteomics* 6, 439–450.
- Davies RB (1987). Hypothesis testing when a nuisance parameter is present only under the alternative. *Biometrika* 74, 33–43.
- Deng C, Xiong X, Krutchinsky AN (2009). Unifying fluorescence microscopy and mass spectrometry for studying protein complexes in cells. *Mol Cell Proteomics* 8, 1413–1423.
- Emsley P, Cowtan K (2004). Coot: model-building tools for molecular graphics. *Acta Crystallogr D Biol Crystallogr* 60, 2126–2132.
- Fadri M, Daquinag A, Wang S, Xue T, Kunz J (2005). The pleckstrin homology domain proteins Slm1 and Slm2 are required for actin cytoskeleton organization in yeast and bind phosphatidylinositol-4,5-bisphosphate and TORC2. *Mol Biol Cell* 16, 1883–1900.
- Finn RD *et al.* (2010). The Pfam protein families database. *Nucleic Acids Res* 38, D211–D222.
- Frohlich F, Moreira K, Aguilar PS, Hubner NC, Mann M, Walter P, Walther TC (2009). A genome-wide screen for genes affecting eisosomes reveals Nce102 function in sphingolipid signaling. *J Cell Biol* 185, 1227–1242.
- Frost A, Perera R, Roux A, Spasov K, Destaing O, Egelman EH, De Camilli P, Unger VM (2008). Structural basis of membrane invagination by F-BAR domains. *Cell* 132, 807–817.



- Frost A, Unger VM, De Camilli P (2009). The BAR domain superfamily: membrane-molding macromolecules. *Cell* 137, 191–196.
- Grossmann G, Malinsky J, Stahlschmidt W, Loibl M, Weig-Meckl I, Frommer WB, Opekarova M, Tanner W (2008). Plasma membrane microdomains regulate turnover of transport proteins in yeast. *J Cell Biol* 183, 1075–1088.
- Grossmann G, Opekarova M, Malinsky J, Weig-Meckl I, Tanner W (2007). Membrane potential governs lateral segregation of plasma membrane proteins and lipids in yeast. *EMBO J* 26, 1–8.
- Guindon S, Gascuel O (2003). A simple, fast, and accurate algorithm to estimate large phylogenies by maximum likelihood. *Syst Biol* 52, 696–704.
- Ho Y *et al.* (2002). Systematic identification of protein complexes in *Saccharomyces cerevisiae* by mass spectrometry. *Nature* 415, 180–183.
- Ito T, Chiba T, Ozawa R, Yoshida M, Hattori M, Sakaki Y (2001). A comprehensive two-hybrid analysis to explore the yeast protein interactome. *Proc Natl Acad Sci USA* 98, 4569–4574.
- Itoh T, Erdmann KS, Roux A, Habermann B, Werner H, De Camilli P (2005). Dynamin and the actin cytoskeleton cooperatively regulate plasma membrane invagination by BAR and F-BAR proteins. *Dev Cell* 9, 791–804.
- Johannes L, Mayor S (2010). Induced domain formation in endocytic invagination, lipid sorting, and scission. *Cell* 142, 507–510.
- Jones DT, Taylor WR, Thornton JM (1992). The rapid generation of mutation data matrices from protein sequences. *Comput Appl Biosci* 8, 275–282.
- Krogan NJ *et al.* (2006). Global landscape of protein complexes in the yeast *Saccharomyces cerevisiae*. *Nature* 440, 637–643.
- Lee E, Marcucci M, Daniell L, Pypaert M, Weisz OA, Ochoa GC, Farsad K, Wenk MR, De Camilli P (2002). Amphiphysin 2 (Bin1) and T-tubule biogenesis in muscle. *Science* 297, 1193–1196.
- Lingwood D, Simons K (2010). Lipid rafts as a membrane-organizing principle. *Science* 327, 46–50.
- Longtine MS, McKenzie A 3rd, Demarini DJ, Shah NG, Wach A, Brachat A, Philippsen P, Pringle JR (1998). Additional modules for versatile and economical PCR-based gene deletion and modification in *Saccharomyces cerevisiae*. *Yeast* 14, 953–961.
- Luo G, Gruhler A, Liu Y, Jensen ON, Dickson RC (2008). The sphingolipid long-chain base-Pkh1/2-Ypk1/2 signaling pathway regulates eisosome assembly and turnover. *J Biol Chem* 283, 10433–10444.
- Malinska K, Malinsky J, Opekarova M, Tanner W (2003). Visualization of protein compartmentation within the plasma membrane of living yeast cells. *Mol Biol Cell* 14, 4427–4436.
- Mann HB, Whitney DR (1947). On a test of whether one of two random variables is stochastically larger than the other. *Ann Math Stat* 18, 50–60.
- Marchler-Bauer A *et al.* (2007). CDD: a conserved domain database for interactive domain family analysis. *Nucleic Acids Res* 35, D237–D240.
- Markin VS (1981). Lateral organization of membranes and cell shapes. *Biophys J* 36, 1–19.
- Marti-Renom MA, Stuart AC, Fiser A, Sanchez R, Melo F, Sali A (2000). Comparative protein structure modeling of genes and genomes. *Annu Rev Biophys Biomol Struct* 29, 291–325.
- Masuda M, Mochizuki N (2010). Structural characteristics of BAR domain superfamily to sculpt the membrane. *Semin Cell Dev Biol* 21, 391–398.
- Moreira KE, Walther TC, Aguilar PS, Walter P (2009). Pil1 controls eisosome biogenesis. *Mol Biol Cell* 20, 809–818.
- Munro S (2003). Lipid rafts: elusive or illusive? *Cell* 115, 377–388.
- Notredame C, Higgins DG, Heringa J (2000). T-Coffee: a novel method for fast and accurate multiple sequence alignment. *J Mol Biol* 302, 205–217.
- Pandit SB, Gosar D, Abhiman S, Sujatha S, Dixit SS, Mhatre NS, Sowdhamini R, Srinivasan N (2002). SUPFAM—a database of potential protein superfamily relationships derived by comparing sequence-based and structure-based families: implications for structural genomics and function annotation in genomes. *Nucleic Acids Res* 30, 289–293.
- Peter BJ, Kent HM, Mills IG, Vallis Y, Butler PJ, Evans PR, McMahon HT (2004). BAR domains as sensors of membrane curvature: the amphiphysin BAR structure. *Science* 303, 495–499.
- Phair RD, Gorski SA, Misteli T (2004). Measurement of dynamic protein binding to chromatin in vivo, using photobleaching microscopy. *Methods Enzymol* 375, 393–414.
- Poveda JA, Fernandez AM, Encinar JA, Gonzalez-Ros JM (2008). Protein-promoted membrane domains. *Biochim Biophys Acta* 1778, 1583–1590.
- Roux A, Cuvelier D, Nassoy P, Prost J, Bassereau P, Goud B (2005). Role of curvature and phase transition in lipid sorting and fission of membrane tubules. *EMBO J* 24, 1537–1545.
- Russell RB, Barton GJ (1992). Multiple protein sequence alignment from tertiary structure comparison: assignment of global and residue confidence levels. *Proteins* 14, 309–323.
- Sadreyev RI, Baker D, Grishin NV (2003). Profile-profile comparisons by COMPASS predict intricate homologies between protein families. *Protein Sci* 12, 2262–2272.
- Sircar A, Chaudhury S, Kilambi KP, Berrondo M, Gray JJ (2010). A generalized approach to sampling backbone conformations with RosettaDock for CAPRI rounds 13–19. *Proteins* 78, 3115–3123.
- Soding J (2005). Protein homology detection by HMM-HMM comparison. *Bioinformatics* 21, 951–960.
- Stimpson HE, Toret CP, Cheng AT, Pauly BS, Drubin DG (2009). Early-arriving Syp1p and Ede1p function in endocytic site placement and formation in budding yeast. *Mol Biol Cell* 20, 4640–4651.
- Stradalova V, Stahlschmidt W, Grossmann G, Blazikova M, Rachel R, Tanner W, Malinsky J (2009). Furrow-like invaginations of the yeast plasma membrane correspond to membrane compartment of Can1. *J Cell Sci* 122, 2887–2894.
- Tabuchi M, Audhya A, Parsons AB, Boone C, Emr SD (2006). The phosphatidylinositol 4,5-bisphosphate and TORC2 binding proteins Slm1 and Slm2 function in sphingolipid regulation. *Mol Cell Biol* 26, 5861–5875.
- Takei K, Slepnev VI, Haucke V, De Camilli P (1999). Functional partnership between amphiphysin and dynamin in clathrin-mediated endocytosis. *Nat Cell Biol* 1, 33–39.
- Tanos B, Rodriguez-Boulan E (2008). The epithelial polarity program: machineries involved and their hijacking by cancer. *Oncogene* 27, 6939–6957.
- Walther TC, Aguilar PS, Frohlich F, Chu F, Moreira K, Burlingame AL, Walter P (2007). Pkh-kinases control eisosome assembly and organization. *EMBO J* 26, 4946–4955.
- Walther TC, Brickner JH, Aguilar PS, Bernales S, Pantoja C, Walter P (2006). Eisosomes mark static sites of endocytosis. *Nature* 439, 998–1003.
- Youn JY *et al.* (2010). Dissecting BAR domain function in the yeast amphiphysins Rvs161 and Rvs167 during endocytosis. *Mol Biol Cell* 21, 3054–3069.
- Young ME, Karpova TS, Brugger B, Moschenross DM, Wang GK, Schneider R, Wieland FT, Cooper JA (2002). The Sur7p family defines novel cortical domains in *Saccharomyces cerevisiae*, affects sphingolipid metabolism, and is involved in sporulation. *Mol Cell Biol* 22, 927–934.
- Yu H *et al.* (2008). High-quality binary protein interaction map of the yeast interactome network. *Science* 322, 104–110.
- Yu JW, Mendrola JM, Audhya A, Singh S, Keleti D, DeWald DB, Murray D, Emr SD, Lemmon MA (2004). Genome-wide analysis of membrane targeting by *S. cerevisiae* pleckstrin homology domains. *Mol Cell* 13, 677–688.
- Zhang X, Lester RL, Dickson RC (2004). Pil1p and Lsp1p negatively regulate the 3-phosphoinositide-dependent protein kinase-like kinase Pkh1p and downstream signaling pathways Pkc1p and Ypk1p. *J Biol Chem* 279, 22030–22038.